Cell

PcrA Helicase Dismantles RecA Filaments by Reeling in DNA in Uniform Steps

Jeehae Park,[1] Sua Myong,[2] Anita Niedziela-Majka,[4,7] Kyung Suk Lee,[3] Jin Yu,[6] Timothy M. Lohman,[4] and Taekjip Ha[1,2,3,5,*]
[1]Center for Biophysics and Computational Biology
[2]Bioengineering Department
[3]Department of Physics and Center for the Physics of Living Cells
University of Illinois at Urbana-Champaign, Urbana, IL 61801, USA
[4]Department of Biochemistry and Molecular Biophysics, Washington University School of Medicine, St. Louis, MO 63110, USA
[5]Howard Hughes Medical Institute, Urbana, IL 61801, USA
[6]Department of Physics, University of California at Berkeley, Berkeley, CA 94720-7300, USA
[7]Present address: Gilead Sciences Inc., Foster City, CA 94404-1147, USA
*Correspondence: tjha@illinois.edu
DOI 10.1016/j.cell.2010.07.016

SUMMARY

Translocation of helicase-like proteins on nucleic acids underlies key cellular functions. However, it is still unclear how translocation can drive removal of DNA-bound proteins, and basic properties like the elementary step size remain controversial. Using single-molecule fluorescence analysis on a prototypical superfamily 1 helicase, *Bacillus stearothermophilus* PcrA, we discovered that PcrA preferentially translocates on the DNA lagging strand instead of unwinding the template duplex. PcrA anchors itself to the template duplex using the 2B subdomain and reels in the lagging strand, extruding a single-stranded loop. Static disorder limited previous ensemble studies of a PcrA stepping mechanism. Here, highly repetitive looping revealed that PcrA translocates in uniform steps of 1 nt. This reeling-in activity requires the open conformation of PcrA and can rapidly dismantle a preformed RecA filament even at low PcrA concentrations, suggesting a mode of action for eliminating potentially deleterious recombination intermediates.

INTRODUCTION

Helicases are ubiquitous enzymes that are involved in nearly all aspects of nucleic acid metabolism in living organisms (Lohman and Bjornson, 1996; Pyle, 2008; Singleton et al., 2007). Most proteins that belong to this class are also "translocases" that move directionally along a DNA or RNA track, although translocation activity is necessary but not sufficient for duplex DNA unwinding (Lohman et al., 2008; Singleton et al., 2007). In fact, some helicases with demonstrated unwinding activity in vitro may have functions in vivo that do not require unwinding activity. For example, *E. coli* UvrD and yeast Srs2 helicases both display antirecombinase activity that is related to their abilities to displace RecA and RAD51 recombination proteins, respectively, from single-stranded (ss) DNA (Antony et al., 2009; Krejci et al., 2003; Veaute et al., 2003, 2005). Processive translocation and unwinding require repeated cycles of ATP (or other nucleoside triphosphates) hydrolysis that is coupled to directional movement. A key mechanistic question regarding these enzymes concerns the step size taken during translocation and unwinding.

Helicases/translocases belonging to superfamily 1 (SF1) are among the most extensively characterized of these enzymes (Singleton et al., 2007). Rep, PcrA, and UvrD are structurally similar SF1A helicases (Korolev et al., 1997; Lee and Yang, 2006; Singleton et al., 2007; Velankar et al., 1999). The monomeric forms of Rep, UvrD, and PcrA are rapid and highly processive translocases that move with 3′ to 5′ directionality along ssDNA (Brendza et al., 2005; Dillingham et al., 2000, 2002; Fischer et al., 2004; Myong et al., 2005; Niedziela-Majka et al., 2007). Yet, at least a dimeric form of these enzymes is required to unwind duplex DNA processively in vitro (Lohman et al., 2008; Yang et al., 2008; Slatter et al., 2009). Hence, oligomerization and/or interactions with accessory proteins appear to be needed for processive DNA unwinding.

Biochemical studies of PcrA and UvrD monomer translocation on ssDNA have shown that on average one ATP is hydrolyzed per base translocated (Dillingham et al., 2000; Tomko et al., 2007). However, ensemble transient kinetic studies have led to the proposal that UvrD and PcrA monomers translocate with a kinetic step size of ~4 nt (Niedziela-Majka et al., 2007; Tomko et al., 2007). As defined, the kinetic step size provides an estimate of how often a recurrent rate-limiting step takes place during processive movement. Similarly, crystallographic analysis led to the proposal that 1 bp of DNA is unwound per single cycle of ATP hydrolysis (Lee and Yang, 2006), whereas bulk phase (Ali and Lohman, 1997; Yang et al., 2008) as well as single-molecule (Dessinges et al., 2004) kinetic studies indicated that the kinetic step size of unwinding is about 4–6 bp. However, because the kinetic step size estimation relies on the variance measurement, it may be influenced by persistent molecular heterogeneities in the reaction rate within an enzyme population ("static disorder"), which has been observed in single-molecule studies of several enzymes (Adelman et al., 2002; Bianco et al.,

2001; Neuman et al., 2003; Perkins et al., 2004; Spies et al., 2003; Tan et al., 2003; Zhuang et al., 2002). Our single-molecule analysis presented below shows that the translocation rates of single PcrA proteins differ and these differences persist during our observation time window of minutes. When we bypass the complications arising from the static disorder through molecule-by-molecule analysis, the kinetic step size of PcrA translocation on ssDNA is revealed to be 1 nt.

As nonreplicative helicases, the roles of PcrA and UvrD in vivo are yet to be fully defined. PcrA can substitute for several functions of UvrD in vivo whereas Rep cannot (Bidnenko et al., 2006; Lestini and Michel, 2007). One of the suggested functions is removal of RecA at stalled replication forks. UvrD is proposed to act at the fork and remove deleterious RecA filaments formed in the lagging strand. The mechanism by which UvrD (and PcrA) recognizes and functions specifically at the fork structure, given its potential to unwind the template duplex, is unknown.

Using single-molecule FRET (fluorescence resonance energy transfer) analysis (Ha et al., 1996), we discovered that a PcrA monomer induces looping of ssDNA that is tightly coupled to its DNA translocation activity. Looping was observed from the 5′ ssDNA tail of a duplex DNA both in the presence and in the absence of an accompanying 3′ ssDNA tail. In the case of the forked DNA with both tails, contrary to what is expected for a helicase that progresses toward the duplex DNA for its potential unwinding, a PcrA monomer remained in contact with the duplex junction while reeling in the 5′ lagging strand using its motor domains. This robust reeling-in activity could induce efficient displacement of RecA filament displacement from the 5′ tail. Our unexpected findings suggest a mechanism that other superfamily 1 translocases may use to control the potentially toxic recombination intermediates at a stalled replication fork.

RESULTS

PcrA Induces Repetitive Looping of a 5′ ssDNA Tail of a Partial Duplex DNA

B. stearothermophilus PcrA is a 3′–5′ helicase that can unwind a duplex DNA possessing a 3′ single-stranded tail. Because PcrA in vivo would encounter other types of DNA structures such as a forked DNA and a partial duplex DNA with a 5′ ssDNA tail, we examined how PcrA would behave on these DNA structures. To observe PcrA activities on individual DNA molecules, we immobilized DNA on a polyethylene glycol (PEG)-passivated quartz slide via a biotin-neutravidin linkage (Figure 1A) (Ha et al., 2002). A fluorescent donor, Cy3, and an acceptor, Cy5, were attached to the two ends of the single-stranded part so as to report on the time-averaged end-to-end distance of the ssDNA. The ssDNA is highly flexible, with a persistence length on the order of 1–2 nm and with its conformations being averaged on a much faster timescale than our time resolution (30 ms) (Murphy et al., 2004).

When the donor and the acceptor are separated by 40 nt of 5′ tail, $(dT)_{40}$, in a partial duplex (5′pdT40), we observed a FRET efficiency of $E_{FRET} \sim 0.4$ (Figure S1A available online). When PcrA and ATP were added, a gradual FRET increase was detected followed by a rapid drop from individual DNA molecules showing that the 5′ tail end approaches the junction gradually and then is released abruptly (Figure 1B). This asymmetric pattern was repeated multiple times without an observable pause in between and the repetition continued for up to a few minutes. This behavior, which we termed "repetitive cycling," was also observed when the donor and acceptor positions were swapped (Figure S1B) and when a ssDNA of mixed sequence was used (Figure S1C).

The gradual phase of repetitive cycling indicates that two ends of ssDNA are approaching each other gradually. In order to define PcrA's role during this process, first we used the fact that Cy3 becomes brighter in fluorescence when a protein is nearby (Fischer et al., 2004; Myong et al., 2009). This protein-induced fluorescence enhancement is thought to result from protein-induced steric constraints suppressing a nonradiative decay pathway (Aramendia et al., 1994; Luo et al., 2007; Sanborn et al., 2007). When Cy3 is placed at the end of the 5′ tail (with no Cy5 present), its fluorescence intensity rises gradually and drops abruptly in a repetitive manner upon addition of PcrA and ATP (Figure 1C), showing that PcrA is approaching the 5′ end gradually during translocation, consistent with PcrA monomer translocating in a 3′ to 5′ direction (Dillingham et al., 2000, 2002; Niedziela-Majka et al., 2007). In contrast, a substrate that has Cy3 attached at the junction showed no repetitive pattern, indicating that a portion of PcrA remains proximal to the partial duplex junction (Figure 1D, Figure S1D). A corroborating result was obtained in bulk solution where PcrA is added to either of the two Cy3-labeled DNA substrates in a cuvette (Figures S1E and S1F). Only the 5′ tail end-conjugated Cy3 showed a further intensity increase upon ATP addition, suggesting that PcrA maintains contact with the duplex DNA during its translocation toward the 5′ end. The positioning of PcrA at the junction is also supported by an ExoIII footprint assay where the duplex portion is protected from ExoIII degradation in the presence of PcrA and ATP (Figure S1G). We confirmed that repetitive cycling still occurs in the buffer conditions used for ExoIII footprinting (Figure S1H). Finally, Cy3-labeled PcrA showed repetitive FRET changes with the DNA labeled at the 5′ end of the ssDNA tail but not with the DNA labeled at the junction (Figures 2A and 2B), further demonstrating that PcrA maintains contact with the junction during translocation.

The emerging picture is that PcrA can remain anchored to the duplex DNA while using its motor domains to translocate on the 5′ tail, reeling in the 5′ ssDNA tail and progressively extruding a ssDNA loop (Figure 1E). In this model, when PcrA reaches the end and runs off the track, the 5′ tail is rapidly released back to its flexible conformation, immediately followed by the next cycle of PcrA translocation from the junction, resulting in "repetitive looping."

The time PcrA takes for one cycle of looping, Δt, was determined by visually picking the moments of the sharp FRET decrease after the peak value from the standard construct 5′pdT40 (Figure 1F). By plotting the inverse of the average Δt versus ATP concentration and fitting to the Michaelis-Menten equation, we obtained $K_M = 3.5 \pm 0.3$ μM (Figure 1G).

PcrA Reels in ssDNA as a Monomer

To determine the assembly state of PcrA during looping, we conducted several experiments. First, we replaced one native cysteine with alanine (C96A) and conjugated Cy3-maleimide to the remaining cysteine (C247). Upon addition of Cy3-PcrA

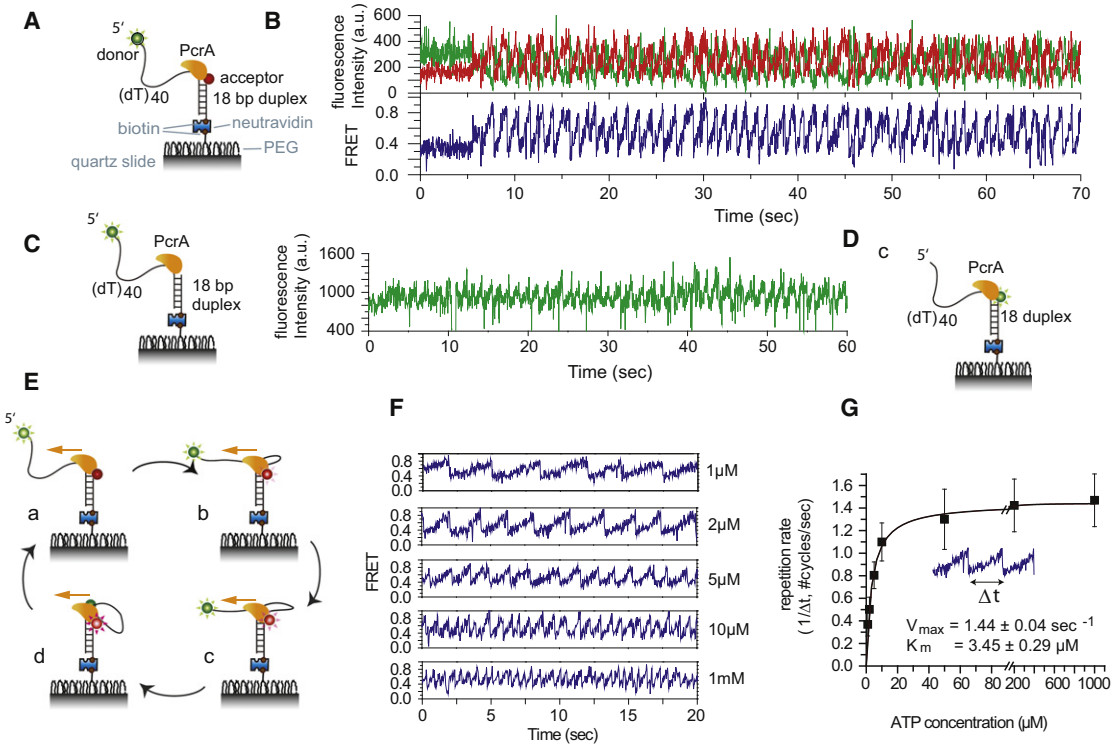

Figure 1. Repetitive Looping of ssDNA Coupled with PcrA Translocation

(A) A dsDNA with 5′$(dT)_{40}$ ssDNA tail is immobilized on a PEG surface via the duplex end.

(B) FRET between the donor (Cy3) and acceptor (Cy5) reports on the change in the time-averaged distance between the tail end and the partial duplex junction. Single-molecule time traces shown (donor intensity in green, acceptor intensity in red, and FRET efficiency in blue) were obtained in the presence of 5 μM ATP and 100 pM PcrA. See also Figures S1A–S1C.

(C) Cy3 intensity increases as PcrA approaches. This property is used to infer distance change between PcrA and the labeled position. Cy3 intensity time trace was obtained under the same conditions as in (A).

(D) When Cy3 was attached to the junction, no periodic intensity fluctuation was observed upon addition of ATP and PcrA. See also Figures S1D–S1H.

(E) Reeling-in model. (a) PcrA binds at 5′ partial duplex junction. (b) Translocation begins in 3′ → 5′ direction while PcrA maintains contact at the junction. (c) ssDNA loop formation and its increase in size as PcrA continues to translocate toward the 5′ end. (d) PcrA reaches the 5′ end and runs off the track. (a)–(d) are repeated over in continual cycles.

(F) Representative FRET time traces of PcrA looping 5′pdT40 at varying ATP concentrations.

(G) Michaelis-Menten fit of repetition rate (1/ < Δt >) versus ATP concentration. Error bars denote standard deviation (SD). Errors in the fit results are shown in standard error of the mean (SEM).

(250 pM) to the surface-immobilized Cy5-labeled DNA, Cy3-PcrA binding was observed to occur in a single step and later followed by a single step disappearance, which is the signature of a monomer (Figures 2A and 2B). In between, asymmetric FRET fluctuations were seen, consistent with repetitive looping for the majority of molecules (85%). Because the PcrA labeling efficiency is ~45%, if two monomers are required for this activity, 20% of the total traces would have shown multiple binding events. None of the time traces showed such behavior. We conclude that a single PcrA monomer is responsible for repetitive looping. Second, we immobilized PcrA with N-terminal hexa-histidines (1 nM) on the surface using biotinylated anti-His-Tag antibody (Figure 2C). Because PcrA is a monomer by itself, PcrA must exist on the surface as isolated monomers. After washing the chamber thoroughly, fluorescently labeled DNA (5′pdT40 without biotin, 0.3 nM) and 1 mM ATP were added. Fluorescence signal appeared as DNA interacted with PcrA immobilized on the surface and more than 65% of DNA molecules showed repetitive looping with an average Δt identical to that of DNA immobilization experiment (Figure 2D). Because PcrA cannot be recruited from solution, we conclude that a PcrA monomer is responsible for repetitive looping. Third, an additional support for monomeric activity came from our binding time analysis (Figure S2A). We recorded FRET signals as we flowed in PcrA and ATP and determined the time it took for repetitive looping to begin for each molecule. The inverse of the average initiation time showed a linear dependence on PcrA concentration (R^2 = 0.95 ± 0.06) as expected for a monomeric activity (Figures S2B–S2I).

ssDNA Length Dependence and PcrA Translocation Rate

We next examined PcrA on pdDNA substrates with 5′ tails of varying lengths (40, 50, 60, 70, and 80 nt) (Figure 3A). The average value of Δt increased linearly with the tail length (Figure 3B), supporting our interpretation that the gradual FRET

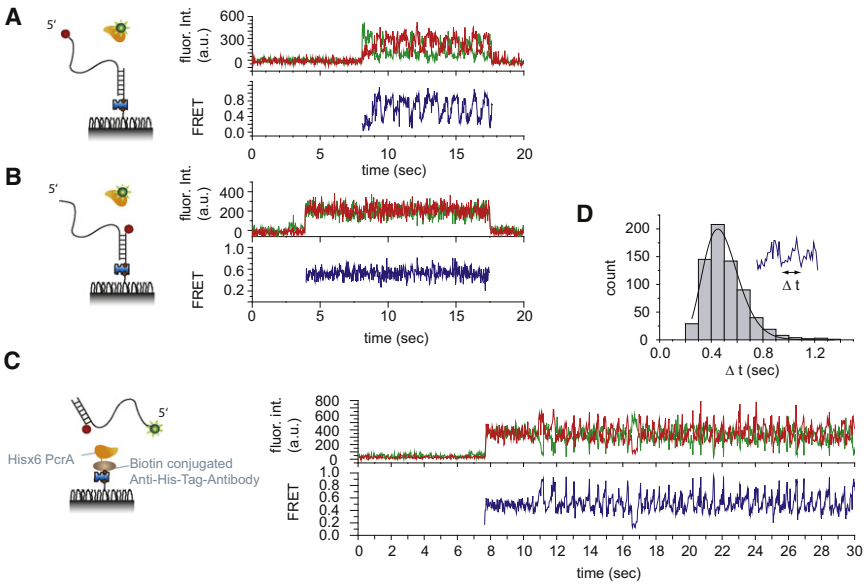

Figure 2. Repetitive Looping Is Induced by a PcrA Monomer

(A) Cy3-labeled PcrA and ATP are added to DNA labeled with Cy5 at the end of the 5′ tail and an example is shown for binding at 8 s, repetitive translocation, and dissociation or photobleaching at 17.7 s.

(B) Cy3-labeled PcrA and ATP are added to DNA labeled with Cy5 at the partial duplex junction. An example trace shows only binding and dissociation but no evidence of relative motion between Cy3 and Cy5.

(C) ATP and Cy3,Cy5-labeled 5′pdT40 DNA are added to PcrA immobilized on the surface via biotinlyated anti-His-tag antibody. An example time trace shows DNA binding at 7.6 s followed by repetitive looping.

(D) Histogram of time interval of repetition (Δt) shown in (C) and a gamma distribution fit.

See also Figure S2.

increase is due to translocation along the 5′ tail and that the abrupt FRET decrease occurs at the end of the ssDNA track. A linear fit to this result shows a translocation rate of 76 ± 5 nt/s, close to those determined in bulk solution under similar but not identical solution conditions (Dillingham et al., 2000, 2002; Niedziela-Majka et al., 2007). The translocation rate is sensitive to the solution conditions. When we used solution conditions that increase the translocation rate of PcrA to

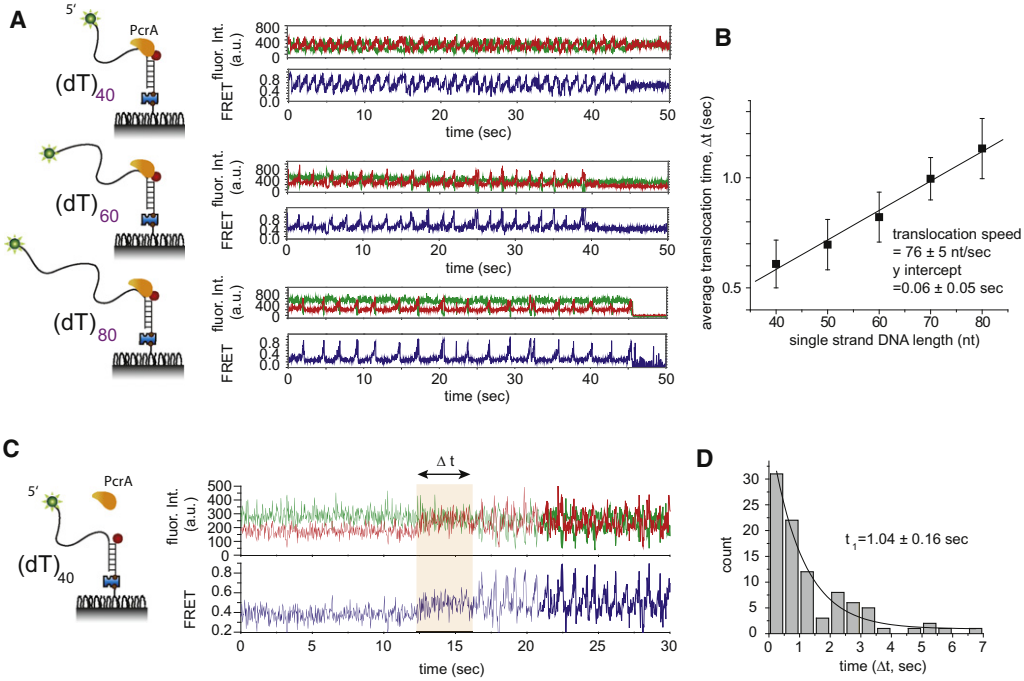

Figure 3. ssDNA Length Dependence and Initiation of Looping

(A) Representative single-molecule FRET time traces of repetitive looping obtained at 5 μM ATP for 5′ ssDNA tails of various lengths. See also Figures S3A–S3E.

(B) Average time of each translocation cycle (<Δt >) versus 5′ tail length at saturating ATP concentration (1 mM). The number of molecules analyzed is as follows with the average number of repetitions per molecule shown in parenthesis: 20 molecules for 5′pdT40 (110), 14 molecules for 5′pdT50 (104), 30 molecules for 5′pdT60 (73), 36 molecules for 5′pdT70 (54), and 34 molecules for 5′pdT80 (48). The error bar denotes SD. Errors in the fit result are in SEM. See also Figure S3F.

(C) Before repetitive looping begins, an elevated FRET plateau is observed.

(D) Histogram of dwell time of the plateau and an exponential fit. The error in the fit result is in SEM.

234 (±2) nt/s on purely ssDNA in bulk solution (Niedziela-Majka et al., 2007), we observed a similarly accelerated translocation rate in our single-molecule measurements with a rate of 231 (±53) nt/s (Figures S3A–S3D). Therefore, the duplex interaction during looping does not appear to affect the overall ssDNA translocation rate of PcrA. In addition, the y intercept of the fit is very close to zero (0.06 ± 0.05), suggesting that PcrA begins to translocate from near the junction and that it reinitiates translocation immediately after release of the 5′ tail. We have also conducted the same measurements and analysis on DNA labeled only with Cy3 (Figures S3E and S3F), and the results agree well with those from the FRET analysis.

Initiation of Looping

From the single-molecule time traces, we could observe the transition from the constant FRET value of DNA-only to the repetitive looping behavior. Interestingly, we detected a transient plateau of slightly elevated FRET value (E_{FRET}~0.5) before repetitive looping begins (Figure 3C). The dwell time histogram of the plateau period could be fitted by an exponential decay with a time constant of 1.0 s (Figure 3D). The molecular details of this initiation step require further investigations.

Kinetic Step Size of PcrA Translocation

Noting the remarkable regularity in repetitive looping, we asked how many rate-limiting steps occur within a single cycle of duration Δt. In general, a larger number of equivalent steps per cycle will result in a sharper Δt histogram. We used the simplest possible model of N irreversible steps connecting the beginning and the end of a cycle.

$$\text{begin} \xrightarrow{k} \xrightarrow{k} \cdots\cdots \xrightarrow{k} \xrightarrow{k} \text{end} \quad (N \text{ steps})$$

In this model, the histogram of Δt should follow the gamma distribution, $(\Delta t)^{N-1} \exp(-k\Delta t)$. Any additional step, for example dissociation at the end of the 5′ end or reinitiation of translocation, with a rate different from k, would only broaden the distribution of Δt. If such an extra step occurs with the same rate as the stepping rate, this analysis will overestimate N only by a factor of 1/N. Therefore, the simplistic model we present here should provide a lower limit on the number of steps involved that is accurate within a few percent.

An important assumption in this analysis is that the translocation process has a defined rate of stepping, k. If static disorder exists in the translocation rate and the Δt histogram is obtained from an ensemble of single molecules, static disorder will increase the width of the distribution, leading to an underestimation of N. To avoid such a problem, we built a Δt histogram from a single PcrA molecule that showed 256 cycles of repetitive looping (Figure 4A). Fitting the single molecule Δt histogram to the gamma distribution yielded N = 34 ± 5 steps for the 40 nt tail, strongly supporting a 1 nt kinetic step size. We also checked if a larger step size, for example, a 4 nt kinetic step size deduced from ensemble kinetic measurements of PcrA and UvrD (Niedziela-Majka et al., 2007; Tomko et al., 2007), still gives a reasonable fit. Fitting the 40 nt tail data by fixing N = 10 (= 40/4) yielded a much poorer fit (Figure 4A).

The same analysis performed on a total of 10 molecules shows that there is a variation of both k and N values among molecules (Figure 4D). In addition, the average of Δt showed significant variation among the molecules as can be seen in the overlay of the gamma distribution fits (Figure 4B). Despite the observed heterogeneity, all molecules showed N larger than 20 for the 40 nt tail (Figure 4C), which is inconsistent with any integer step size larger than 1 nt (Figures 4B–4D). We also observed that N values determined from individual molecules increase as the 5′ tail is increased from 50, 60, 70, to 80 nt without any systematic change in the stepping rate k (Figures 4E, 4F, and 4G). Overall, our data place an upper limit on the kinetic step size consistently smaller than 2 nt, and assuming that there exists a defined integer value for the kinetic step size, the kinetic step size of ssDNA translocation is 1 nt.

Previous ensemble kinetic analyses reported that PcrA and UvrD take average kinetic steps of 4 nt (Niedziela-Majka et al., 2007; Tomko et al., 2007). To test if the observed static disorder in the translocation rate can in principle result in an apparent step size larger than 1 nt, we obtained 9356 Δt values from a population of 77 molecules and built an ensemble histogram (Figure 4H). Due to the heterogeneity, the resulting distribution is broader than that obtained from a single molecule and the fit showed N = 12 for a 40 nt translocation, i.e., 3.3 nt/step. Therefore, kinetic step sizes significantly larger than 1 nt that were estimated from ensemble measurements could be due to the presence of static disorder in the translocation rates among the enzyme population.

PcrA Activity on a Forked DNA

Thus far, we have presented data only on the 5′ partial duplex DNA, which should not be unwound by a 3′ to 5′ helicase. What would happen if a 3′ tail is added in addition to the 5′ tail, that is, will PcrA unwind the duplex DNA instead of displaying translocation on the 5′ tail? We prepared a forked DNA that is identical in structure and fluorescent labeling to the aforementioned 5′-tailed DNA except for the addition of a 20 nt 3′ tail (Figure 5A). If the 18 bp duplex is efficiently unwound by PcrA, the donor-labeled strand should be released from the surface resulting in a decrease of the number of fluorescent spots in the imaging area. Full unwinding was negligible because the number of fluorescent spots per imaging area did not decrease significantly even after 30 min of reaction (Figure 5B). Instead, we observed a robust looping behavior (Figure 5A) likely due to a stable anchoring of PcrA at the duplex junction with concomitant translocation along the 5′ tail. Therefore, a PcrA monomer favors looping of the 5′ tail of a forked DNA over duplex unwinding.

Role of 2B Subdomain and Its Conformation

PcrA and UvrD monomers crystallized with a 3′-tailed partial duplex DNA showed that the 2B subdomain is in contact with the duplex region (Lee and Yang, 2006; Velankar et al., 1999). We hypothesized that this duplex/2B contact may allow PcrA to anchor itself at the junction during translocation and to reinitiate translocation specifically from one end of the ssDNA that is proximal to the junction. We mutated G423 in the 2B subdomain

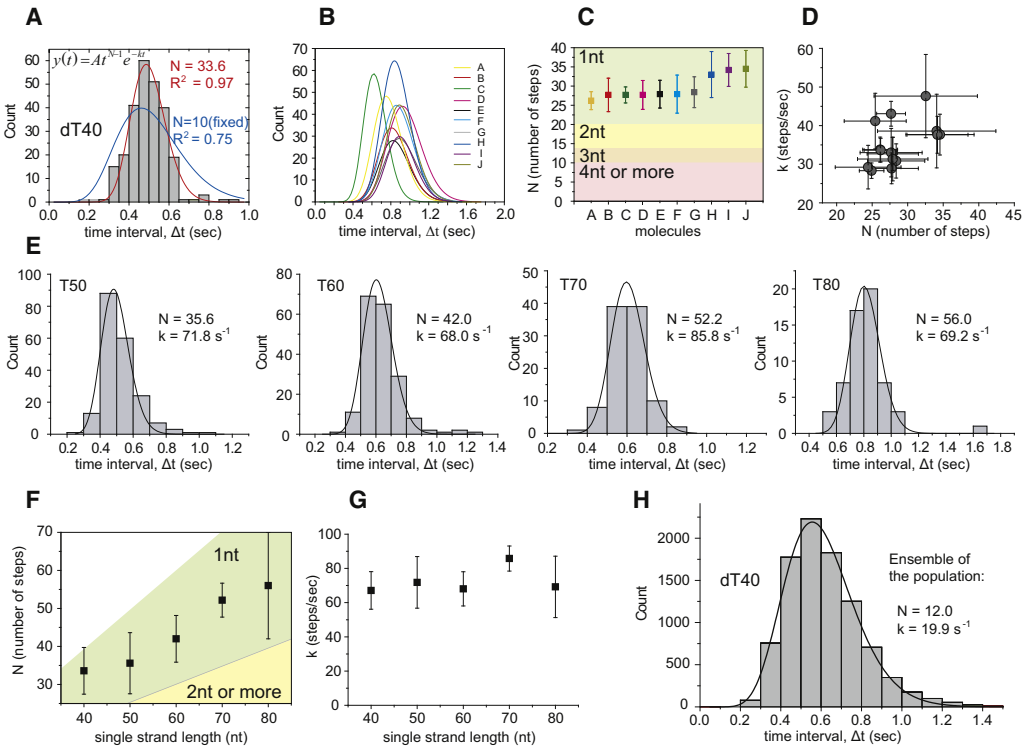

Figure 4. One Nucleotide Kinetic Step Size of Translocation

(A) A Δt histogram obtained from a single PcrA molecule showing 256 repetitive looping events over 140 s. A fit to the gamma distribution is shown in red. Also shown is a fit with the value for N fixed at 10.

(B) Gamma distribution fits of Δt histograms for 10 different PcrA molecules ($R^2 > 0.97$ for each curve). For clarity, the Δt histograms themselves are not shown.

(C) N values determined from 10 different molecules shown in (B) (error bars denote SEM). The molecules (A to J) are ordered with increasing N values. For the 40 nt translocation, the expected zones for kinetic step sizes of 1, 2, 3, and 4 nt are indicated as shades of different color.

(D) Heterogeneity among the PcrA molecules. k versus N for the 10 molecules analyzed in (B) (error bars denote SEM).

(E) Δt histograms and gamma distribution fits obtained from single PcrA molecules on 50, 60, 70, and 80 nt 5′ tail of partial duplex DNA.

(F) N versus ssDNA length for the molecules shown in (A) and (E) (error bars denote SEM).

(G) k versus ssDNA length for the molecules shown in (A) and (E) (error bars denote SEM).

(H) Δt histogram obtained from 77 molecules and gamma distribution fit ($R^2 = 0.99$).

of PcrA, which is the second glycine in the ''GIG box'' that comprises the conserved helix-hairpin-helix motif that contacts the minor groove of the duplex DNA (Figure 5C, Figure S4A). Mutation on the first glycine (G421E) of the GIG box was not viable. On our standard DNA construct (5′pdT40), the G423T mutant showed FRET fluctuations, but these were much less regular than those observed with wild-type PcrA, and the FRET peak values were lower than observed with wild-type (Figures 5Cand 5D). In contrast, mutating T426, which is proximal to the GIG box, to alanine did not cause any change in the looping activity (Figures S4B and S4C). In UvrD, the mutation equivalent to G423T showed a severe decrease in DNA affinity whereas the mutation equivalent to T426A showed only a minor decrease (Lee and Yang, 2006). Therefore, it is likely that PcrA interaction with the duplex via the GIG box of the 2B subdomain is important for the regularity of the looping activity.

The 2B subdomain can swivel between two conformations, termed open and closed (Korolev et al., 1997). To determine the PcrA's conformation during repetitive looping we constructed a PcrA mutant with two cysteines, A533C and C247, that would be in close proximity, ~3.8 nm, in the closed conformation but farther apart, ~5.5 nm, in the open conformation. The mutant was labeled stochastically with a mixture of Cy3 and Cy5 maleimides, and the labeled protein was observed on an unlabeled 5′pdT40 (Figure 5E). Figure 5F shows the initial binding of PcrA to the DNA in the high FRET state, quickly followed by a transition to a low FRET state indicating that PcrA changes its conformation from closed to open at the initial stage of DNA binding and remains in an open conformation during looping (additional examples in Figures S4D–S4F). Intermittent direct excitation of the acceptor showed that the low FRET state is not due to acceptor photobleaching or blinking. Among the 189 molecules analyzed, about 80% exhibited primarily a low FRET state that we assign to the open state (Figure S4G). We conclude that PcrA most likely maintains an open conformation during ssDNA translocation coupled with looping.

PcrA Dismantles a Preformed RecA Filament

Because PcrA shows specificity for binding at a 5′ ssDNA/duplex junction and continuous interaction with the 5′ ssDNA tail, PcrA

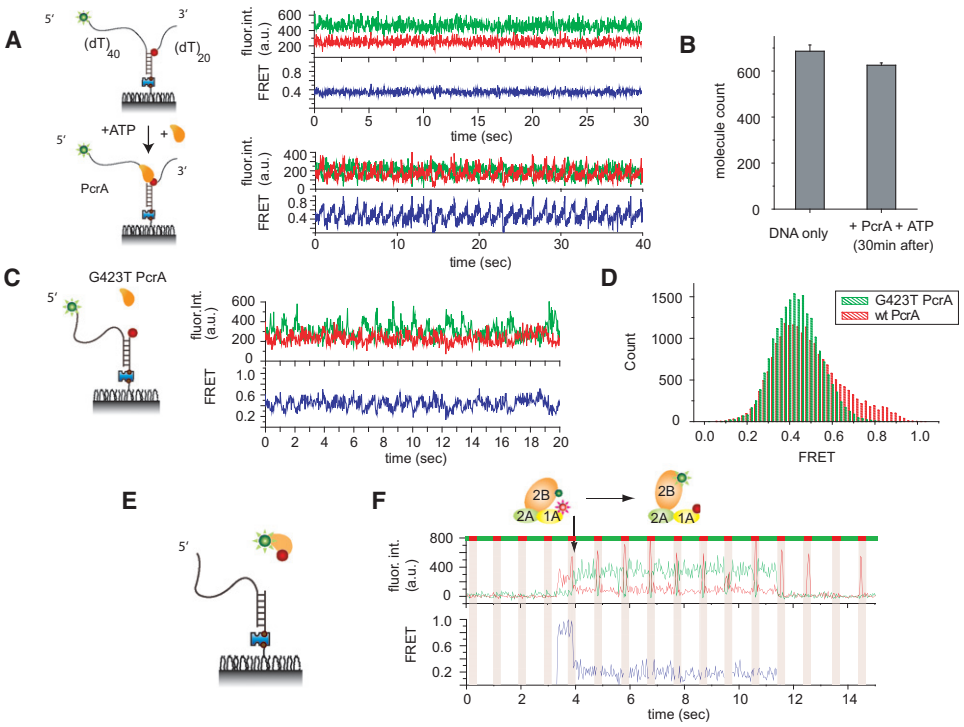

Figure 5. PcrA on a Forked DNA and the Role of 2B Domain of PcrA

(A) A forked DNA substrate labeled with donor and acceptor at the same position as in Figure 1A. A representative set of traces of fluorescence intensities and FRET efficiency are presented before and after adding PcrA (100 pM) and ATP (5 μM).

(B) Number of molecules per imaging area before and after adding PcrA (100 pM) and ATP (1 mM) (error bars denote SD).

(C) Representative time traces of 5′pdT40 in the presence of G423T mutant PcrA and 1 mM ATP. See also Figures S4A–S4C.

(D) FRET values at every time point of the trajectory are collected and plotted into a histogram (wild-type in red, G423T in green).

(E) Dual-labeled PcrA is added to unlabeled 5′pdT40 with 1 mM ATP.

(F) Representative time trace of fluorescence intensities and FRET for dual-labeled PcrA. Every one second, a 0.1 s pulse of red illumination (633 nm) and no green illumination (532 nm) are applied in order to verify the presence of acceptor. Periods of green illumination are marked with green bars and red illumination with red bars above the time traces as well as with shades over the traces. See also Figures S4D–S4G.

may modulate the activity of other proteins that act on the same DNA. In fact, experiments in vivo showed that antirecombinase activity is restored by introducing *Bacillus subtilis* PcrA to a UvrD-deficient strain (Bidnenko et al., 2006; Lestini and Michel, 2007). In order to test if PcrA can counteract RecA by directly destabilizing RecA filaments, we added PcrA to a preformed RecA filament (Figure 6). The RecA filament was formed by incubating 5′pdT40 with RecA and ATP (Figure 6A). With this DNA, filament formation is observed as a FRET decrease (Figure 6B) because RecA binding stretches the ssDNA portion, resulting in an end-to-end distance increase (Joo et al., 2006). RecA filament is formed within 5 min and a steady state is reached (Figures S5A–S5C). Ten minutes after the RecA addition (250 nM), 1 nM PcrA is introduced while keeping the free RecA and ATP levels in solution constant. A significant portion (>50%) of the low FRET DNA population moved to higher FRET values, indicating that RecA is removed (Figures 6C and 6D). The equilibrium population of DNA that is occupied by RecA further decreased at higher PcrA concentration (Figures 6D and 6F). The new equilibrium induced by PcrA could be reached very rapidly, with more than half the reaction completed in less than 0.5 min (Figure 6E, Figures S5D–S5F).

We could also observe the real-time progress of RecA filament dissociation followed by PcrA-induced looping (Figure 6G). Upon adding PcrA to a preformed RecA filament, we observe a phase in which slow looping occurs several times, 20 s to 40 s (the slowness is likely due to competition with RecA), which transitions to fast repetitive looping (at ~60 s and beyond) when PcrA temporarily triumphs over RecA. During this fast looping period, the looping rates are comparable to that on bare DNA, suggesting that RecA is fully removed (Figure S5G). It is likely that a pseudo-equilibrium is reached where RecA rebinding competes with PcrA in a concentration-dependent manner such that FRET time traces show dynamic changes between fast looping, slow looping, and no looping periods (Figure S5H). Our data overall suggest that a PcrA monomer's looping/translocation activities can efficiently dismantle preformed RecA filaments.

DISCUSSION

Function and the Conformation of the 2B Subdomain

The role of the 2B subdomain in SF1 helicases has been controversial. Because of its interaction with the duplex in the crystal structures, it was once thought that the 2B subdomain acts to

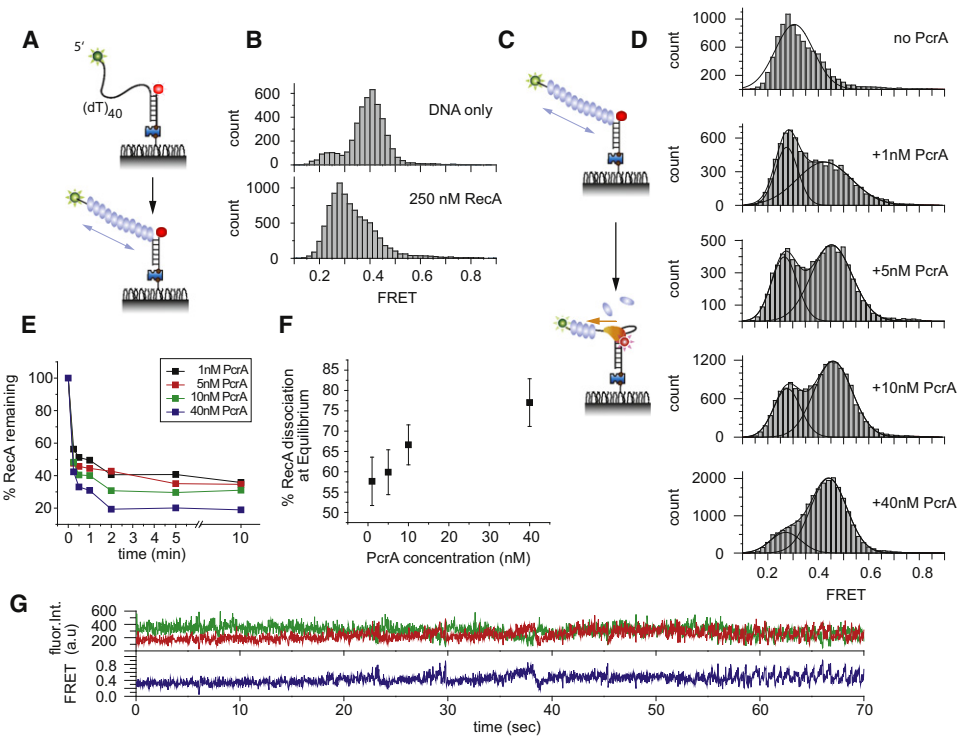

Figure 6. RecA Filament Removal by PcrA

(A and B) 5′pdT40 DNA is preincubated with 250 μM RecA and 1 mM ATP for 5 min. FRET histograms are shown before and after incubation. See also Figures S5A–S5C.

(C and D) 1–40 nM PcrA is then added to the preformed RecA filament maintaining ATP and RecA concentration constant in solution. FRET histograms were obtained 10 min after PcrA addition. See also Figure S5D.

(E) Fraction of RecA remaining versus time for different PcrA concentration conditions. See also Figures S5E and S5F.

(F) Fraction of DNA molecules that lost RecA filament 10 min after PcrA addition (error bars denote SEM from the exponential fit of Figure 6E).

(G) Representative time traces of fluorescence intensities and FRET efficiency upon adding 1 nM PcrA addition to the preformed RecA filament. See also Figures S5G and S5H.

destabilize the duplex and helps the unwinding process. However, deletion of the 2B subdomain actually enhances the unwinding activity of Rep (Brendza et al., 2005; Cheng et al., 2002). The looping activity of PcrA that we discovered on 5′-tailed partial duplex DNA requires tight binding to the duplex junction via an anchor subdomain in the helicase. The anchor is likely provided by the 2B subdomain because when the GIG box in the 2B subdomain is perturbed by mutation, PcrA lost its ability to pull ssDNA all the way to the end of the track. Such an interaction would be suitable for recognizing stalled replication forks or gapped duplexes.

The 2B subdomain has been found in two different orientations, open and closed, for Rep, PcrA, and UvrD. In the closed conformation of PcrA (Figure 7A) (Velankar et al., 1999), the 5′ ssDNA tail would need to traverse approximately 34 Å to enter the 1A domain with the correct orientation (Figure 7C), whereas our tail length-dependent data suggest that translocation begins very close to the duplex region. It is thus likely that the 2B orientation of PcrA during looping differs from what is observed in the PcrA (and UvrD) crystal structures, and our single-molecule data indeed indicate that the 2B subdomain takes an open conformation.

We used structural modeling to test if the open conformation would allow a proper engagement with the 5′ tail. We started with the closed form of the PcrA structure (Protein Data Bank ID 3pjr) and rotated the 2B subdomain together with the 3′-tailed DNA by 130°, to mimic the open conformation of Rep (PDB ID 1uaa) (Figure 7B). This resulted in the 3′ tail being positioned in an incorrect polarity relative to the ssDNA-binding site of the protein (Figure 7D). Interestingly, however, the 5′ end of the duplex is in proximity to the ssDNA-binding sites (8.5 Å between F192 and the first base of the 5′ DNA end). As a result, an extended 5′ tail could now interact with the ssDNA-binding site of the translocase with the correct polarity starting from F192. As translocation proceeds along the 5′ tail, the ssDNA would be reeled in through the 2A subdomain and then through the 1A subdomain (Figure 7E). A single-stranded loop would form behind F192 and grow without steric constraints as translocation continues. We also confirmed that PcrA binds to the 5′ tail with the correct polarity (Figure S6). Overall, our data and structural modeling suggest that an open conformation is indeed the functional conformation necessary for the reeling-in activity of PcrA.

PcrA Translocation Mechanism

Stopped-flow studies with reaction synchronization and single turnover experimental design suggested a 4 nt kinetic step size

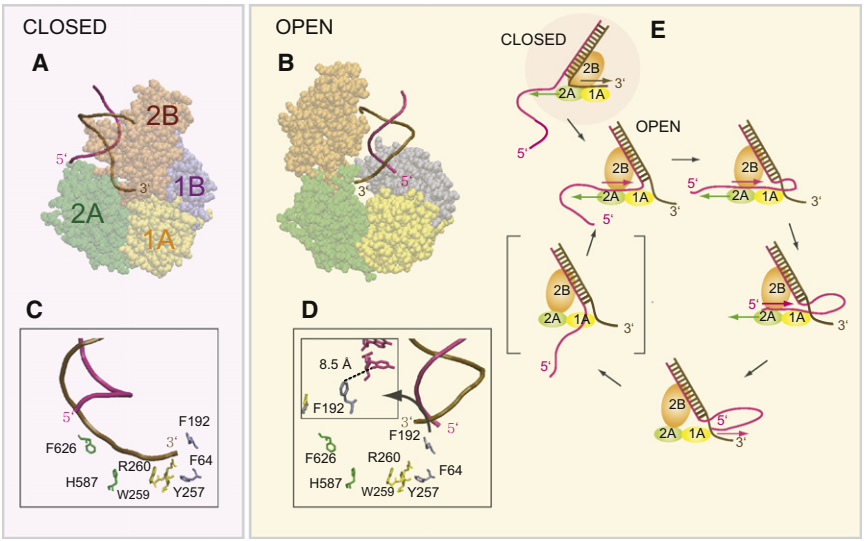

Figure 7. Structural Model of PcrA Translocation on 5′ ssDNA of Partial Duplex

(A) Crystal structure of PcrA in closed form in complex with a 3′-tailed partial duplex DNA. PcrA is in the Van der Waals representation with the domains colored individually in yellow (1A), green (2A), purple (1B), and orange (2B). DNA is presented with two colors for each strand: brown (3′ tail strand) and pink (5′ complementary strand).

(B) Open form of PcrA generated by 130° rotation of 2B domain together with DNA from the structure shown in (A).

(C) The ssDNA-binding sites of PcrA in the closed form as shown in (A). Each protein residue is colored according to the color scheme of the domain it belongs to.

(D) The ssDNA-binding sites of PcrA in the open form as shown in (B). Color schemes are the same as those used in (C). Inset shows an enlarged image of the region around 5′ end of the DNA placed in proximity to F192.

(E) PcrA translocation model at the DNA fork. The closed form of PcrA is shown inside the pink circle. Others are in the open form. Movement of PcrA is indicated with green arrows. The relative movement of the 5′ ssDNA tail (pink) is shown with pink arrow.

See also Figure S6.

for both PcrA and UvrD (Fischer et al., 2004; Niedziela-Majka et al., 2007; Tomko et al., 2007). Combined with the 1:1 ratio between translocation and ATP hydrolysis (Tomko et al., 2007), it was proposed that PcrA and UvrD translocate via a nonuniform stepping mechanism wherein they move about 4 nt very rapidly using 1 ATP per nt, then pause momentarily before taking the next four steps.

However, the ensemble studies used to estimate the kinetic step size were based on variance analysis that is intrinsically susceptible to any static disorder, and they were analyzed with the necessary assumption (Fischer et al., 2004; Tomko et al., 2007) that all molecules in the sample share the same average reaction rate. This assumption, however, is not possible to validate in ensemble studies, and the first single-molecule helicase study already showed that another SF1 helicase, RecBCD, can display a high degree of variation in the DNA unwinding rate among nominally identical RecBCD molecules (Bianco et al., 2001). We found that the PcrA translocase also displays significant static disorder in its translocation rate on ssDNA, although the origin of this behavior is not currently understood. Therefore, to avoid complications arising from static disorder, a variance-based analysis should be performed on *a single molecule*.

Our discovery that when PcrA initiates translocation from a ss-ds DNA junction it undergoes repetitive looping of DNA that repeats more than 100 times has provided an ideal platform for determining the kinetic step size from a single molecule, not a collection of single molecules. Our analysis shows that PcrA should translocate with a tight coupling of 1 nt translocated per 1 ATP hydrolyzed and that there is no additional hierarchy of larger steps or pauses for ssDNA translocation.

Implications for the Kinetic Step Size of Duplex Unwinding

The variance-based method used to estimate the kinetic step size was originally developed for studies of DNA unwinding by UvrD (Ali and Lohman, 1997) and was subsequently adopted for other helicases including RecBCD (Lucius et al., 2002), NPH-II (Jankowsky et al., 2000), *E. coli* DnaB helicase (Galletto et al., 2004), T7 helicase (Jeong et al., 2004), *E. coli* RecBC (Wu and Lohman, 2008), hepatitis C virus NS3 (Raney and Benkovic, 1995; Serebrov and Pyle, 2004), T4 Dda (Eoff and Raney, 2006), and NS3h (Levin et al., 2004) and also for single-molecule analysis of UvrD (Dessinges et al., 2004). In all of these studies except for DnaB, kinetic step sizes of unwinding that are significantly larger than 1 bp were reported. Our results here suggest that the presence of static disorder in the unwinding rates can lead to an overestimation of the kinetic step size. Because a direct detection of unwinding steps or a thorough evaluation of static disorder in the unwinding rate are lacking for these helicases except for NS3, we cannot yet conclude whether unwinding by these helicases occurs in steps larger than 1 bp or not. However, a translocation step size of 1 nt does not necessarily mean that unwinding occurs in 1 bp steps because NS3 helicase unwinds DNA (Myong et al., 2007) and RNA (Dumont et al., 2006) in ~3 bp increments even though its translocation along the DNA backbone likely occurs in 1 nt steps (Myong et al., 2007).

Functional Implications of ssDNA Looping by PcrA

The results reported here, along with previous structural and biochemical studies, suggest that a PcrA monomer can bind to a twin-tailed DNA fork in two modes. In one mode it can bind to the leading 3′ ssDNA strand and the duplex as in the crystal

structures. In the second mode it can bind to the 5′ ssDNA and the duplex, and in this mode it can reel in the 5′ ssDNA tail using a looping mechanism. The persistent interaction of a PcrA monomer with the 5′ tail of a forked DNA construct suggests that the PcrA monomer looping activity may compete with and thus inhibit DNA unwinding at a fork even at higher PcrA concentrations that support processive unwinding. In fact, a study has shown that an ~10-fold higher concentration of *Staphylococcus aureus* PcrA was needed to unwind a forked DNA compared to a 3′ partial duplex (Anand and Khan, 2004). Unwinding activity of UvrD on a forked structure was also shown to be lower relative to a 3′ ssDNA structure (Ali et al., 1999).

UvrD can help restart replication by Tus removal (Bidnenko et al., 2006) and dismantle recombination intermediates from a ssDNA gap on the lagging strand of a blocked replication fork (Lestini and Michel, 2007). Interestingly, *Bacillus subtilis* PcrA, but not Rep, is capable of substituting for UvrD in both of these activities. Our finding that a PcrA monomer can stably anchor itself on the duplex while actively translocating along the 5′ tail provides a plausible mechanism for stripping deleterious RecA filaments from the lagging strand (Flores et al., 2005; Lestini and Michel, 2007; Morel et al., 1993; Veaute et al., 2005; Zieg et al., 1978). Previous studies in vitro showed that UvrD induced removal of RecA filaments on circular ssDNA that lacks dsDNA (Veaute et al., 2005), and over 100 nM of UvrD and a 15 min reaction were required to observe effective RecA removal. In our experiments, using partial duplex DNA molecules, however, we observed effective RecA removal at PcrA concentrations as low as 1 nM and within 30 s showing that the anti-RecA activity conserved in PcrA is much more effective in the context of a 5′ ss-ds DNA junction, likely mediated by interactions with the duplex. This activity is distinct from that of Rep, which interferes with the formation of RecA filament but does not dismantle the preformed filament (Myong et al., 2005).

EXPERIMENTAL PROCEDURES

PcrA Reaction Conditions

Standard reaction buffer was 20 mM Tris-HCl, pH 8.0, 10 mM KCl, 5 mM $MgCl_2$,with an oxygen scavenging system (1 mg/ml glucose oxidase, 0.4% (w/v) D-glucose, 0.04 mg/ml catalase, and 1% v/v 2-mercaptoethanol). The measurements were performed at room temperature (21°C ± 1°C). One millimolar ATP was used in all experiments unless specified otherwise. *Bacillus stearothermophilus* PcrA, purified as described (Niedziela-Majka et al., 2007), was first mixed at 100 pM with reaction buffer and added to a flow chamber that had 100 pM DNA specifically immobilized on a PEG-coated quartz surface through biotin-neutravidin linkage (Ha et al., 2002).

Single-Molecule Experiments

Prism type total internal reflection microscopy was used to acquire single-molecule data. A Nd:YAG laser with 532 nm wavelength was guided through the prism to generate an evanescent field of illumination. A water-immersion objective (60×, numerical aperture 1.2, Olympus) was used to collect the signal and the scattered light was removed using a 550 nm long-pass filter. Cy3 and Cy5 signals were separated using a 630 nm dichroic mirror and sent to the CCD camera (iXon DV 887-BI, Andor Technology). Data were recorded as a stream of imaging frames and analyzed with scripts written in IDL to generate fluorescence intensity time trajectories of individual molecules. A time resolution of 0.03 s was used.

Data Analysis

Singe-molecule fluorescence time trajectories were viewed and analyzed using programs written with Matlab. FRET efficiency, E_{FRET}, was approximated as the ratio between the acceptor intensity and the sum of the acceptor and donor intensities after correction for the crosstalk between the two detection channels. Peak-to-peak analysis to obtain Δt was measured manually from individual FRET time trajectories aided with a program written in Matlab and the resulting histograms were fitted using Origin. Standard 0.1 s binning was used for fitting to the gamma distribution because varying the binning size did not change the fitting result significantly.

SUPPLEMENTAL INFORMATION

Supplemental Information includes Extended Experimental Procedures and six figures and can be found with this article online at doi:10.1016/j.cell.2010.07.016.

ACKNOWLEDGMENTS

We thank C. Joo, R. Roy, M. Schlierf, S. Syed, M.C. McKinney, M.K. Nahas, B. Okumus, S.A. McKinney, E. Bozek, and J.D. Smith for experimental help; S. Arslan, J. Yodh, H. Balci, I. Cisse, B.C. Stevens, G. Lee, M. Brenner, E. Tomko, C. Fischer, and M. Spies for helpful discussion; I. Cann and his lab for providing *Staphylococcus aureus* PcrA for the initial studies; R. Pugh for help on ExoIII footprint assay; M. Schlierf, J. Yodh, H. Balci, and E. Tomko for careful reading of the manuscript. Funds were provided by the National Institutes of Health (GM-065367 to T.H. and GM-045948 to T.M.L.) and by the National Science Foundation (0822613 and 0646550 to T.H.). T.H. is an investigator with the Howard Hughes Medical Institute.

Received: December 11, 2008
Revised: February 2, 2010
Accepted: July 8, 2010
Published: August 19, 2010

REFERENCES

Adelman, K., La Porta, A., Santangelo, T.J., Lis, J.T., Roberts, J.W., and Wang, M.D. (2002). Single molecule analysis of RNA polymerase elongation reveals uniform kinetic behavior. Proc. Natl. Acad. Sci. USA *99*, 13538–13543.

Ali, J.A., and Lohman, T.M. (1997). Kinetic measurement of the step size of DNA unwinding by Escherichia coli UvrD helicase. Science *275*, 377–380.

Ali, J.A., Maluf, N.K., and Lohman, T.M. (1999). An oligomeric form of E. coli UvrD is required for optimal helicase activity. J. Mol. Biol. *293*, 815–834.

Anand, S.P., and Khan, S.A. (2004). Structure-specific DNA binding and bipolar helicase activities of PcrA. Nucleic Acids Res. *32*, 3190–3197.

Antony, E., Tomko, E.J., Xiao, Q., Krejci, L., Lohman, T.M., and Ellenberger, T. (2009). Srs2 disassembles Rad51 filaments by a protein-protein interaction triggering ATP turnover and dissociation of Rad51 from DNA. Mol. Cell *35*, 105–115.

Aramendia, P.F., Negri, R.M., and Sanroman, E. (1994). Temperature-dependence of fluorescence and photoisomerization in symmetrical carbocyanines - influence of medium viscosity and molecular-structure. J. Phys. Chem. *98*, 3165–3173.

Bianco, P.R., Brewer, L.R., Corzett, M., Balhorn, R., Yeh, Y., Kowalczykowski, S.C., and Baskin, R.J. (2001). Processive translocation and DNA unwinding by individual RecBCD enzyme molecules. Nature *409*, 374–378.

Bidnenko, V., Lestini, R., and Michel, B. (2006). The Escherichia coli UvrD helicase is essential for Tus removal during recombination-dependent replication restart from Ter sites. Mol. Microbiol. *62*, 382–396.

Brendza, K.M., Cheng, W., Fischer, C.J., Chesnik, M.A., Niedziela-Majka, A., and Lohman, T.M. (2005). Autoinhibition of Escherichia coli Rep monomer helicase activity by its 2B subdomain. Proc. Natl. Acad. Sci. USA *102*, 10076–10081.

Cheng, W., Brendza, K.M., Gauss, G.H., Korolev, S., Waksman, G., and Lohman, T.M. (2002). The 2B domain of the Escherichia coli Rep protein is not required for DNA helicase activity. Proc. Natl. Acad. Sci. USA *99*, 16006–16011.

Dessinges, M.N., Lionnet, T., Xi, X.G., Bensimon, D., and Croquette, V. (2004). Single-molecule assay reveals strand switching and enhanced processivity of UvrD. Proc. Natl. Acad. Sci. USA *101*, 6439–6444.

Dillingham, M.S., Wigley, D.B., and Webb, M.R. (2000). Demonstration of unidirectional single-stranded DNA translocation by PcrA helicase: measurement of step size and translocation speed. Biochemistry *39*, 205–212.

Dillingham, M.S., Wigley, D.B., and Webb, M.R. (2002). Direct measurement of single-stranded DNA translocation by PcrA helicase using the fluorescent base analogue 2-aminopurine. Biochemistry *41*, 643–651.

Dumont, S., Cheng, W., Serebrov, V., Beran, R.K., Tinoco, I., Jr., Pyle, A.M., and Bustamante, C. (2006). RNA translocation and unwinding mechanism of HCV NS3 helicase and its coordination by ATP. Nature *439*, 105–108.

Eoff, R.L., and Raney, K.D. (2006). Intermediates revealed in the kinetic mechanism for DNA unwinding by a monomeric helicase. Nat. Struct. Mol. Biol. *13*, 242–249.

Fischer, C.J., Maluf, N.K., and Lohman, T.M. (2004). Mechanism of ATP-dependent translocation of E.coli UvrD monomers along single-stranded DNA. J. Mol. Biol. *344*, 1287–1309.

Flores, M.J., Sanchez, N., and Michel, B. (2005). A fork-clearing role for UvrD. Mol. Microbiol. *57*, 1664–1675.

Galletto, R., Jezewska, M.J., and Bujalowski, W. (2004). Unzipping mechanism of the double-stranded DNA unwinding by a hexameric helicase: quantitative analysis of the rate of the dsDNA unwinding, processivity and kinetic step-size of the Escherichia coli DnaB helicase using rapid quench-flow method. J. Mol. Biol. *343*, 83–99.

Ha, T., Enderle, T., Ogletree, D.F., Chemla, D.S., Selvin, P.R., and Weiss, S. (1996). Probing the interaction between two single molecules: fluorescence resonance energy transfer between a single donor and a single acceptor. Proc. Natl. Acad. Sci. USA *93*, 6264–6268.

Ha, T., Rasnik, I., Cheng, W., Babcock, H.P., Gauss, G.H., Lohman, T.M., and Chu, S. (2002). Initiation and re-initiation of DNA unwinding by the Escherichia coli Rep helicase. Nature *419*, 638–641.

Jankowsky, E., Gross, C.H., Shuman, S., and Pyle, A.M. (2000). The DExH protein NPH-II is a processive and directional motor for unwinding RNA. Nature *403*, 447–451.

Jeong, Y.J., Levin, M.K., and Patel, S.S. (2004). The DNA-unwinding mechanism of the ring helicase of bacteriophage T7. Proc. Natl. Acad. Sci. USA *101*, 7264–7269.

Joo, C., McKinney, S.A., Nakamura, M., Rasnik, I., Myong, S., and Ha, T. (2006). Real-time observation of RecA filament dynamics with single monomer resolution. Cell *126*, 515–527.

Korolev, S., Hsieh, J., Gauss, G.H., Lohman, T.M., and Waksman, G. (1997). Major domain swiveling revealed by the crystal structures of complexes of *E. coli* Rep helicase bound to single-stranded DNA and ADP. Cell *90*, 635–647.

Krejci, L., Van Komen, S., Li, Y., Villemain, J., Reddy, M.S., Klein, H., Ellenberger, T., and Sung, P. (2003). DNA helicase Srs2 disrupts the Rad51 presynaptic filament. Nature *423*, 305–309.

Lee, J.Y., and Yang, W. (2006). UvrD helicase unwinds DNA one base pair at a time by a two-part power stroke. Cell *127*, 1349–1360.

Lestini, R., and Michel, B. (2007). UvrD controls the access of recombination proteins to blocked replication forks. EMBO J. *26*, 3804–3814.

Levin, M.K., Wang, Y.H., and Patel, S.S. (2004). The functional interaction of the hepatitis C virus helicase molecules is responsible for unwinding processivity. J. Biol. Chem. *279*, 26005–26012.

Lohman, T.M., and Bjornson, K.P. (1996). Mechanisms of helicase-catalyzed DNA unwinding. Annu. Rev. Biochem. *65*, 169–214.

Lohman, T.M., Tomko, E.J., and Wu, C.G. (2008). Non-hexameric DNA helicases and translocases: mechanisms and regulation. Nat. Rev. Mol. Cell Biol. *9*, 391–401.

Lucius, A.L., Vindigni, A., Gregorian, R., Ali, J.A., Taylor, A.F., Smith, G.R., and Lohman, T.M. (2002). DNA unwinding step-size of E. coli RecBCD helicase determined from single turnover chemical quenched-flow kinetic studies. J. Mol. Biol. *324*, 409–428.

Luo, G., Wang, M., Konigsberg, W.H., and Xie, X.S. (2007). Single-molecule and ensemble fluorescence assays for a functionally important conformational change in T7 DNA polymerase. Proc. Natl. Acad. Sci. USA *104*, 12610–12615.

Morel, P., Hejna, J.A., Ehrlich, S.D., and Cassuto, E. (1993). Antipairing and strand transferase activities of E. coli helicase II (UvrD). Nucleic Acids Res. *21*, 3205–3209.

Murphy, M.C., Rasnik, I., Cheng, W., Lohman, T.M., and Ha, T. (2004). Probing single-stranded DNA conformational flexibility using fluorescence spectroscopy. Biophys. J. *86*, 2530–2537.

Myong, S., Rasnik, I., Joo, C., Lohman, T.M., and Ha, T. (2005). Repetitive shuttling of a motor protein on DNA. Nature *437*, 1321–1325.

Myong, S., Bruno, M.M., Pyle, A.M., and Ha, T. (2007). Spring-loaded mechanism of DNA unwinding by hepatitis C virus NS3 helicase. Science *317*, 513–516.

Myong, S., Cui, S., Cornish, P.V., Kirchhofer, A., Gack, M.U., Jung, J.U., Hopfner, K.P., and Ha, T. (2009). Cytosolic viral sensor RIG-I is a 5′-triphosphate-dependent translocase on double-stranded RNA. Science *323*, 1070–1074.

Neuman, K.C., Abbondanzieri, E.A., Landick, R., Gelles, J., and Block, S.M. (2003). Ubiquitous transcriptional pausing is independent of RNA polymerase backtracking. Cell *115*, 437–447.

Niedziela-Majka, A., Chesnik, M.A., Tomko, E.J., and Lohman, T.M. (2007). Bacillus stearothermophilus PcrA monomer is a single-stranded DNA translocase but not a processive helicase in vitro. J. Biol. Chem. *282*, 27076–27085.

Perkins, T.T., Li, H.W., Dalal, R.V., Gelles, J., and Block, S.M. (2004). Forward and reverse motion of single RecBCD molecules on DNA. Biophys. J. *86*, 1640–1648.

Pyle, A.M. (2008). Translocation and unwinding mechanisms of RNA and DNA helicases. Annu. Rev. Biophys. *37*, 317–336.

Raney, K.D., and Benkovic, S.J. (1995). Bacteriophage T4 Dda helicase translocates in a unidirectional fashion on single-stranded DNA. J. Biol. Chem. *270*, 22236–22242.

Sanborn, M.E., Connolly, B.K., Gurunathan, K., and Levitus, M. (2007). Fluorescence properties and photophysics of the sulfoindocyanine Cy3 linked covalently to DNA. J. Phys. Chem. B *111*, 11064–11074.

Serebrov, V., and Pyle, A.M. (2004). Periodic cycles of RNA unwinding and pausing by hepatitis C virus NS3 helicase. Nature *430*, 476–480.

Singleton, M.R., Dillingham, M.S., and Wigley, D.B. (2007). Structure and mechanism of helicases and nucleic acid translocases. Annu. Rev. Biochem. *76*, 23–50.

Slatter, A.F., Thomas, C.D., and Webb, M.R. (2009). PcrA helicase tightly couples ATP hydrolysis to unwinding double-stranded DNA, modulated by the initiator protein for plasmid replication, RepD. Biochemistry *48*, 6326–6334.

Spies, M., Bianco, P.R., Dillingham, M.S., Handa, N., Baskin, R.J., and Kowalczykowski, S.C. (2003). A molecular throttle: the recombination hotspot chi controls DNA translocation by the RecBCD helicase. Cell *114*, 647–654.

Tan, E., Wilson, T.J., Nahas, M.K., Clegg, R.M., Lilley, D.M., and Ha, T. (2003). A four-way junction accelerates hairpin ribozyme folding via a discrete intermediate. Proc. Natl. Acad. Sci. USA *100*, 9308–9313.

Tomko, E.J., Fischer, C.J., Niedziela-Majka, A., and Lohman, T.M. (2007). A nonuniform stepping mechanism for *E. coli* UvrD monomer translocation along single-stranded DNA. Mol. Cell *26*, 335–347.

Veaute, X., Jeusset, J., Soustelle, C., Kowalczykowski, S.C., Le Cam, E., and Fabre, F. (2003). The Srs2 helicase prevents recombination by disrupting Rad51 nucleoprotein filaments. Nature *423*, 309–312.

Veaute, X., Delmas, S., Selva, M., Jeusset, J., Le Cam, E., Matic, I., Fabre, F., and Petit, M.A. (2005). UvrD helicase, unlike Rep helicase, dismantles RecA nucleoprotein filaments in Escherichia coli. EMBO J. *24*, 180–189.

Velankar, S.S., Soultanas, P., Dillingham, M.S., Subramanya, H.S., and Wigley, D.B. (1999). Crystal structures of complexes of PcrA DNA helicase with a DNA substrate indicate an inchworm mechanism. Cell *97*, 75–84.

Wu, C.G., and Lohman, T.M. (2008). Influence of DNA end structure on the mechanism of initiation of DNA unwinding by the Escherichia coli RecBCD and RecBC helicases. J. Mol. Biol. *382*, 312–326.

Yang, Y., Dou, S.X., Ren, H., Wang, P.Y., Zhang, X.D., Qian, M., Pan, B.Y., and Xi, X.G. (2008). Evidence for a functional dimeric form of the PcrA helicase in DNA unwinding. Nucleic Acids Res. *36*, 1976–1989.

Zhuang, X., Kim, H., Pereira, M.J., Babcock, H.P., Walter, N.G., and Chu, S. (2002). Correlating structural dynamics and function in single ribozyme molecules. Science *296*, 1473–1476.

Zieg, J., Maples, V.F., and Kushner, S.R. (1978). Recombinant levels of Escherichia coli K-12 mutants deficient in various replication, recombination, or repair genes. J. Bacteriol. *134*, 958–966.